Journal of Solid State Chemistry 202 (2013) 15–21

Contents lists available at SciVerse ScienceDirect

Journal of Solid State Chemistry

journal homepage: www.elsevier.com/locate/jssc

Magnetic structures in RNi_4B (R=Nd, Tb, Ho, Er)

E. Alleno [a,*], C. Mazumdar [b]

[a] ICMPE, UMR 7182 CNRS-UPEC, 2 rue Henri Dunant, 94320 Thiais, France
[b] Saha Institute of Nuclear Physics, Sector-1, Block-AF, 700064 Kolkata, India

ARTICLE INFO

Article history:
Received 12 December 2012
Received in revised form
22 February 2013
Accepted 1 March 2013
Available online 13 March 2013

Keywords:
Rare earth intermetallics
Ferromagnetism
Neutron scattering
Crystal electric field

ABSTRACT

Neutron diffraction has been performed on RNi_4B (R=Nd, Tb, Ho, Er) polycrystals. The orthorhombic structure for NdNi4B and the $CeCo_4B$ structure type (hexagonal) for $TbNi_4B$ and $HoNi_4B$ are confirmed. Our data also show that this last structure is currently the best approximant for $ErNi_4B$. The RNi_4B (R=Nd, Tb, Ho, Er) order ferromagnetically at respectively 11.0, 18.1, 6.2 and 10.0 K. The crystal electric field (CEF) interaction controls the magnetic anisotropy in this series leading to an easy axis ~30 deg above the basal plane in RNi_4B (R=Nd, Tb, Ho) and parallel to the c-axis in $ErNi_4B$ at 1.6 K. The RNi_4B (R=Nd, Tb, Ho) display a spin re-orientation below T_c which arises from a competition between the second order term and the higher order terms of the CEF hamiltonian.

1. Introduction

The compounds forming in the $CaCu_5$ type of structure (space group $P6/mmm$) and their derivatives have been studied for a long time due to various interesting phenomena. Out of these compounds, the RCo_5 (R=rare earth) may get a special mention for their magnetic properties leading to $SmCo_5$ as an excellent material for high-coercivity magnet applications [1,2] and the RNi_5 for their hydrogen absorption capabilities leading to Ni-MH battery applications [3,4]. In contrast to the RCo_5 compounds where Co atoms are a primary contributor to magnetism, the magnetic properties of the RNi_5 compounds are quite different. Unlike Co in RCo_5, the Ni atoms ($2c$ and $3g$ sites) in RNi_5 are non-magnetic [5–9,10,11] either because the Ni d-band is almost filled or because the exchange is too weak to polarize sufficiently the d-band. As a result, the source of magnetism in the RNi_5 compounds is the rare-earth ($1a$ site) and the R–R indirect exchange interaction (RKKY). Only this results in ferromagnetic ordering at quite low temperatures (33 K in $GdNi_5$) [12]. The interaction between the rare-earth 4f electrons and the crystal electric field (CEF) controls the magnetic anisotropy of these compounds. In RNi_5 (R=Nd, Ho), the a axis is the easy magnetization axis [6,8,10,11,13,14] while in RNi_5 (R=Sm, Er, Tm) the easy axis is the c axis [5,7,9]. This is in agreement with the sign of the Stevens coefficient of the rare-earth (α_J) [15] when considering a negative sign for the second order CEF parameter V_2^0 across the whole series of compounds. $TbNi_5$ exhibits a more complex behavior with an incommensurate fan-like structure with two wave vectors (q_1=(0, 0, 0) and q_2=(0, 0, 0.019)) [16] for magnetic fields smaller than 400 Oe [17] and a fully ferromagnetic structure for H > 400 Oe [16].

In the RCo_5 and RNi_5 compounds, the substitution of the transition metal by other 3d-elements (Mn, Fe, Cu) or light elements (B, Al, C, Si) leads to modified hydrogen absorption capabilities and/or modified magnetic properties. The RNi_4B compounds are such examples with on the one side, reduced hydrogen absorption capacity and thus no interest for this purpose [18] and on the other side, more complex magnetic behaviors. The RNi_4B with magnetic rare-earths display a ferromagnetic ground state with Curie temperatures in the same range (4–36 K) [19–27] as in the RNi_5 series (T_c=36 K in $GdNi_4B$) except in $SmNi_4B$ where T_c is anomalously large (T_c=39 K) [21,24,28]. This last compound also exhibits a large magnetic hysteresis due to the presence of mono-atomic like domain layers [28].

Given the experimental magnetization results [19–27] and the similarities between the RNi_4B and the RNi_5, it is very unlikely that in the ferromagnetic RNi_4B compounds, the Ni atoms carry a "large" ($>0.5\ \mu_B$) magnetic moment. However, the question of a "small" magnetic moment ($<0.1\ \mu_B$) on the Ni atoms has been raised theoretically and experimentally in these compounds. Band structure calculations reveal that the total density of states at the Fermi level contain mainly 3d-states of Ni atoms [29]. Such calculations are supported by valence band XPS spectra on several members of the RNi_4B family [29–34]. Spin-resolved band structure calculations suggest weak Ni-3d ferromagnetism with an ordered nickel moment of 0.08 μ_B at 0 K in $GdNi_4B$. [35,36]. Experimentally, YNi_4B which incidentally led to the discovery of the superconducting RNi_2B_2C borocarbides [37,38], exhibits a Pauli paramagnetic behavior with an effective paramagnetic moment of 0.24 μ_B per formula

* Corresponding author. Fax: +33 1 49 78 12 03.
E-mail address: eric.alleno@icmpe.cnrs.fr (E. Alleno).

0022-4596/$ - see front matter © 2013 Elsevier Inc. All rights reserved.
http://dx.doi.org/10.1016/j.jssc.2013.03.003

unit without any magnetic ordering [39]. Similarly, a Magnetic X-Ray Circular Dichroism study [40] on intermediate valence $CeNi_4B$ [21,23,32,41,42] did not reveal a spontaneous Ni moment: only a very small ~0.01 μ_B nickel moment could be observed under a 4 T field. All these results points to an enhanced paramagnetic behavior or at most, to a very weak ferromagnetic behavior of the magnetic Ni sub-system in the RNi_4B series. Since the limit of detection of a moment measured by neutron powder diffraction is at most 0.2–0.3 μ_B/ atom, we will not draw any conclusion on this subject. We simply considered the possibility of a Ni moment in the RNi_4B compounds in the process of Rietveld refining our neutron data for the sake of completeness. We obtained values of Ni moment $|\mu_{Ni}| \leq 0.2\mu_B \pm 0.07\mu_B$ smaller than the detection limit and this is consistent with experiments and calculations reported in literature [19–27,35,36,39,40].

Substitution of nickel by boron also brings structural complexity in the RNi_4B. This series of compounds was initially thought to be isostructural to the hexagonal $CeCo_4B$ type of structure (space group $P6/mmm$) (see e.g., [43]), where the rare earth atoms occupy the 1*a* (0, 0, 0) and 1*b* (0, 0, 1/2) sites (labeled R1a and R1b hereafter), nickel atoms occupy the 2*c* (1/3, 2/3,0) and 6i (1/2, 0, 0.28) sites (labeled Ni2*c* and Ni6*i*) while boron atoms occupy the 2d (1/3, 2/3, 1/2) position (see Fig. 1, top panels). However, it was later observed that for several members of this series, the $CeCo_4B$ unit cell can only be considered as a subcell. For example, diffraction patterns could only be respectively indexed in a 3-fold, 6-fold and 8-fold supercell in the cases of YNi_4B [44], $LaNi_4B$ [44], and $CeNi_4B$ [45]. The complete structure of annealed YNi_4B (nominal) [46] and as-cast $NdNi_4B$ [47] were subsequently solved by single crystal techniques and these works confirmed that the $CeCo_4B$ structure is only an approximant for these compounds. The case of $ErNi_4B$ is more controversial: as-cast $ErNi_4B$ (nominal) was found to crystallize in a complex hexagonal structure [48] similar to that of YNi_4B while more recently, annealed $ErNi_4B$ was found to crystallize in the simple $CeCo_4B$ structure [49].

In the literature, all the conventional magnetization and susceptibility measurements were carried out on polycrystalline RNi_4B. The knowledge of the magnetocrystalline anisotropy is thus currently poor and we thought that a neutron diffraction experiment would be a good means of gaining information on this matter. In this work, we report on the first direct measurement of the magnetic structures of some members of the RNi_4B (R=Nd, Tb, Ho, and Er) series of compounds using enriched ^{11}B. Neutron diffraction helped us to confirm the crystallographic structure of RNi_4B (R=Nd, Tb, Ho) and a ferromagnetic ordering for all of them. The easy magnetization axis was determined and it shows a common trend with the homologous RNi_5 series of compounds. However, unlike in the RNi_5 series, a spin-reorientation of the rare-earth moments occurs for R=Nd, Tb, Ho analogs as temperature is varied below T_c.

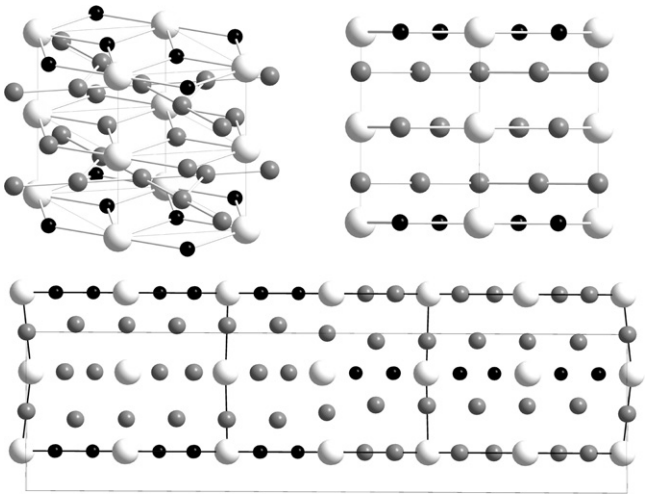

Fig. 1. Comparison between the $TbNi_4B$ ($CeCo_4B$ type) and $NdNi_4B$ structures. White spheres: Tb atoms; gray spheres: Ni atoms; black spheres: B atoms. Top left panel: extended hexagonal unit cell (thin gray lines) of $TbNi_4B$; extra atoms selected from neighboring cells to match part of the $NdNi_4B$ larger unit cell; arbitrarily chosen in-plane bonds represented by thick white lines. Top right panel: same extended $TbNi_4B$ hexagonal unit cell projected along the [1 −1 0] direction. Bottom panel: extended $(1 \times 1.5 \times 1)$ orthorhombic $NdNi_4B$ unit cell projected along the [1 0 0] direction to better understand its relation to the $TbNi_4B$ structure. The thin lines represent the $NdNi_4B$ unit cell. The thick lines represent the same or similar extended $TbNi_4B$ unit cell as in the top panels.

2. Experimental

Every compound was melted in an induction furnace under vacuum. Stochiometric amounts of Nd, Tb, Ho, Er (> 99.9%), Ni (> 99.9%) and ^{11}B (Eurisotop, 99.8% chemically pure, 97.5% isotopically enriched) were used to synthesize the compounds. The ingots thus obtained were flipped-over and melted several times to achieve homogeneity. Weight loss ranged from 0 ($NdNi_4B$) to 30 mg ($HoNi_4B$) for 12 g samples. No annealing was carried out neither after melting nor after powdering. The composition of the resultant materials was checked by carrying out powder X-ray diffraction (XRD) at room temperature using a Bruker D8 diffractometer (Cu $K\alpha$ radiation). The neutron diffraction experiments were carried out at the neutron powder diffractometer beamline D1B at Institut Laue-Langevin (ILL) in Grenoble, France, using the wavelength of 2.52 Å. The sample was held in a cylindrical vanadium can in a cryostat and was measured as a function of temperature [1.5–35 K] in the angular range of 5 to 85°. The patterns were recorded in constant temperature mode after a stabilization time of 5 minutes. Rietveld refinements of both the X-ray as well as the neutron diffraction pattern were carried out using the program FULLPROF [50]. Because of the presence of 2.5% of ^{10}B, the neutron linear absorption coefficient (μR) was computed according to Ref. [51]: the values are reported in Table 1. The scale factor, the profile parameters, the lattice parameters and the magnetic moments were refined parameters. The atomic coordinates, the site occupation factors and thermal displacement parameters were held fixed. The profile reliability factor and the integrated intensity reliability factor are hereby respectively noted R_p and R_I.

3. Results

3.1. Crystallographic structures

$TbNi_4B$ is reported to form in the hexagonal $CeCo_4B$ type of structure (space group $P6/mmm$) [52]. A very good agreement was obtained by Rietveld refining the room temperature XRD pattern of $TbNi_4B$ with this structure. No secondary phase peak could be

Table 1
Parameters relevant to the magnetic Rietveld refinements (Fig. 4) of the neutron patterns measured at 1.6 K in the ferromagnetic state. Neutron absorption coefficient (μR), moment per rare atom (μ_R), angle (θ) between the moment direction and the *c*-axis of the hexagonal unit cell ($CeCo_4B$) or the *b*-axis of the orthorhombic unit-cell ($NdNi_4B$, marked with*), profile reliability factor (R_p) and integrated intensity reliability factor (R_I).

RNi_4B	μR	μ_R (μ_B)	θ (deg)	R_p (%)	R_I (%)
Nd	1.0	3.1(1)	59(4)*	3.1	9.0
Tb	0.8	5.7(1)	62(2)	3.0	6.0
Ho	1.0	6.7(1)	62(2)	3.1	2.4
Er	1.45	8.7	0	4.9	7.0

detected and we obtained $a=4.992(1)$ Å and $c=6.945(1)$ Å as lattice parameters at 300 K, in good agreement with published values [49,52]. The good quality of the neutron pattern refinement ($R_p=3.2\%$ and $R_I=7.9\%$) shown in Fig. 2a confirms the $CeCo_4B$ type of structure for $TbNi_4B$ with $a=4.97(1)$ Å and $c=6.92(1)$ Å at 33 K.

$HoNi_4B$ is also reported to form in the hexagonal $CeCo_4B$ type of structure [53,54]. A good agreement was obtained by refining the room temperature XRD pattern of $HoNi_4B$ with this structure and we obtained $a=4.967(1)$ Å and $c=6.937(1)$ Å as lattice parameters at room temperature. However faint peaks (4% in intensity of the largest peak in the pattern) were left unindexed and after adding 2% (mass fraction) Ho_2O_3 and 1% (mass fraction) $Ho_2Ni_{21}B_6$ [55] as secondary phases, only three faint peaks remained unindexed. The corresponding peaks were also left unindexed in the neutron pattern (19 K) and attempts to index these peaks with other known structures of the RNi_4B, e.g. the $Y_{0.9}Ni_{4.1}B$ [46] and $Er_{0.9}Ni_{4.1}B$ [48] structure types degraded the reliability factors. This strongly suggests that these faint peaks belong to an unknown impurity phase. We hence further proceeded using the $CeCo_4B$ type of structure for $HoNi_4B$. The resulting refinement of the neutron pattern ($R_p=3.4\%$; $R_I=11.0\%$) is shown in Fig. 2.b and we obtained $a=4.96(1)$ Å and $c=6.92(1)$ Å as lattice parameters at 19 K.

$ErNi_4B$ is reported to crystallize either in the hexagonal $CeCo_4B$ [49] or in the more complex $Er_{0.9}Ni_{4.1}B$ [48] structure types. This last structure ($P6/mmm$, $a=14.840$ Å, $c=6.919$ Å) derives from the simpler $CeCo_4B$ by tripling the lattice parameter a, keeping c constant and by partially replacing erbium atoms by nickel atoms. We refined our XRD pattern with the two structure types and obtained the following lattice parameters and reliability factors:

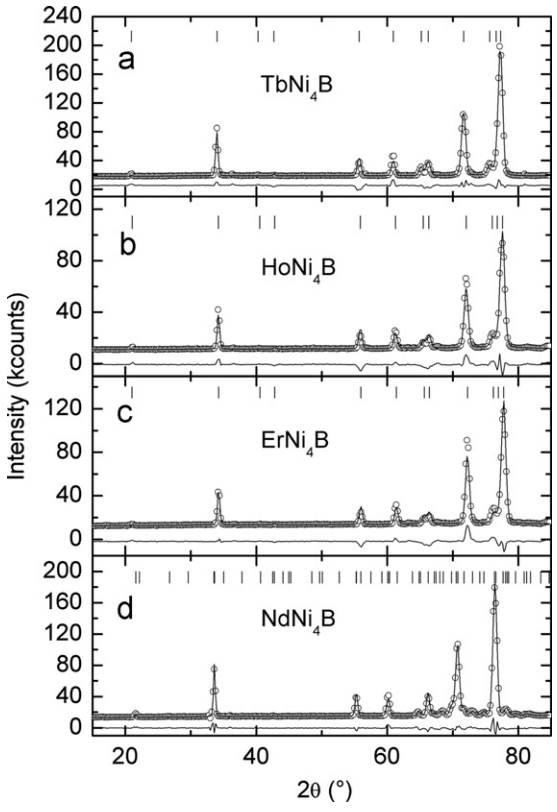

Fig. 2. Rietveld refinement of the neutron pattern of $TbNi_4B$, $HoNi_4B$ and $ErNi_4B$ respectively at 33 K, 19 K, 24 K (paramagnetic state) using the hexagonal $CeCo_4B$ structure type. Panel a: $TbNi_4B$; panel b: $HoNi_4B$; panel c: $ErNi_4B$. Panel d: Rietveld refinement of the neutron pattern of $NdNi_4B$ at 24 K (paramagnetic state) using the complex orthorhombic structure described in Ref. [47]. Faint peaks characteristic of this structure can be noticed in the angular range [65–80 deg]. The open circles are the experimental data, the line is the calculated pattern, the bottom line is the difference pattern (exp.–calc.) and the upper ticks are the Bragg angles.

$a=4.957(1)$ Å, $c=6.932(1)$ Å; $R_p=11.7\%$, $R_I=11.9\%$ for the $CeCo_4B$ structure type and $a=14.870(2)$ Å, $c=6.931(1)$ Å; $R_p=20.9\%$, $R_I=29.7\%$ for the $Er_{0.9}Ni_{4.1}B$ structure type. A similar work was carried out for the neutron pattern measured at 24K (paramagnetic state): $R_p=3.5\%$, $R_I=14.6\%$ and $R_p=5.6\%$, $R_I=28.4\%$ were respectively obtained for the $CeCo_4B$ structure type and for the $Er_{0.9}Ni_{4.1}B$ structure type. The fairly good agreement between the calculated neutron pattern with the $CeCo_4B$ structure type and the experimental neutron pattern measured at 24 K can be seen in Fig. 2c. These results strongly suggest that the $Er_{0.9}Ni_{4.1}B$ structure type [48] is not a good description of the structure of $ErNi_4B$. Few faint lines were left unindexed in the XRD pattern by the $CeCo_4B$ structure and similarly to $HoNi_4B$, after adding 2% Er_2O_3 and 1% $Er_2Ni_{21}B_6$ [55] as secondary phases, three to four weak lines (3% in intensity of the largest peak of the pattern) remained unindexed. Some of these remaining lines could indeed be indexed by taking the larger hexagonal unit cell of the $Er_{0.9}Ni_{4.1}B$ structure. We thus considered the possibility of dimorphism in our sample, e.g. a mixture of the $CeCo_4B$-type and $Er_{0.9}Ni_{4.1}B$-type of structures which might originate from differing cooling rates in the induction furnace. A refinement of the XRD pattern led to only marginal improvements of the reliability factors ($R_p=11.4\%$; $R_I=10.9\%$ for the $CeCo_4B$ structure type; $R_I=21.5\%$ for the $Er_{0.9}Ni_{4.1}B$ structure) with poor agreement between the experimental and calculated intensity of the remaining lines. Moreover, this fit indicated that at most, only a small amount of $Er_{0.9}Ni_{4.1}B$ phase (13% mass fraction) might be present in our sample. Given these uncertainties, we think that the simple hexagonal $CeCo_4B$ structure type is currently the best approximation to the structure of $ErNi_4B$, but we cannot conclude as in Ref. [49] that it crystallizes in the $CeCo_4B$ structure type.

Because of the preceding $ErNi_4B$ case, we also attempted in a preliminary trial to refine the XRD pattern of $NdNi_4B$ using the $CeCo_4B$ structure type. But several peaks remained unindexed (18% in intensity of the largest peak) showing that the $CeCo_4B$ structure is not relevant in this case. In fact the orthorhombic unit cell corresponding to the more complex structure reported by Salamakha et al. [47] (space group $Imma$, $Z=12$, $a=5.057$ Å, $b=6.980$ Å, $c=26.271$ Å) was required to index every XRD peak, leaving no unindexed peak. A representation of this structure is shown in Fig. 1 (bottom panel). Its unit cell (a, b, c) derives from the hexagonal $CeCo_4B$ unit cell (a_0, b_0, c_0) with $a=a_0$, $b=c_0$ and c parallel to a_0+b_0 with $c=3a_0\sqrt{3}$. In fig. 1, along the orthorhombic c-axis, one can find three contiguous hexagonal unit cells deriving from the $CeCo_4B$ unit cell: the left one is very close to the $CeCo_4B$ structure and only differs by the positions of the Ni atoms in the Ni layer; the right one derives from the left one by shifting its atom positions by a vector $1/2c_0=1/2b$; the central one is a mixture of the half the left and half the right hexagonal unit cell. Moreover, the Ni layers are no more located in a single plane but are rippled. The peak positions and intensities of the XRD data of $NdNi_4B$ taken at 300 K were very well matched by this orthorhombic structure, leaving no peak unindexed and the lattice parameters thus obtained are $a=5.052(1)$ Å, $b=6.974(1)$ Å, and $c=26.251(3)$ Å, in good agreement with the published values. As in the case of the powder XRD pattern of this compound, several weak neutron lines of the "high temperature" neutron pattern cannot be indexed using the $CeCo_4B$ hexagonal cell. Our neutron data were also satisfactorily refined ($R_p=2.9\%$ and $R_I=5.7\%$) by the structure reported by Salamakha et al. [47] as exemplified in Fig. 1d by the 24 K pattern (paramagnetic state) which yielded $a=5.02(1)$ Å, $b=6.95(1)$ Å, and $c=26.21(1)$ Å. This confirms that $NdNi_4B$ crystallizes in this orthorhombic structure.

3.2. Magnetic structures

The neutron diffraction measurements carried out on the RNi_4B compounds (Nd, Tb, Ho, Er) only showed a major enhancement of

some peak intensities for the patterns taken below their respective magnetic transition temperatures. The absence of any additional peaks clearly indicates that no change of the unit cell occurs on magnetic ordering. Rietveld refinements and comparison with magnetization measurements showed that only a ferromagnetic arrangement of the rare-earth moments is compatible with the neutron patterns.

3.2.1. $TbNi_4B$

The difference between the pattern taken at the lowest temperature of our experiment, e.g. 1.6 K and the pattern taken at 35 K is shown in Fig. 3 for $TbNi_4B$. It completely can be indexed with the $CeCo_4B$ unit cell as expected for a ferromagnetically ordered compound. The observation of the (00l) peaks in the difference pattern of $TbNi_4B$ indicates that the moments make an angle θ with the c-axis at 1.6 K. With neutron powder diffraction, we cannot determine the orientation of the component of the moment parallel to the (a, b) hexagonal plane. But in analogy with what is observed in $TbNi_5$ [11], we refined the pattern with the moments parallel to the a-axis. We initially assumed that the rare earth atoms bear the same moment on both the R1a and R1b sites. For the sake of completeness, we considered the possibility of a magnetic moment on the nickel atoms (both Ni2c and Ni6i sites). We obtained $\mu_{Ni2c}=+0.0\pm0.07\ \mu_B$, $\mu_{Ni6i}=-0.2\pm0.06\ \mu_B$, and this shows that if the nickel sites bear a moment, it is smaller than 0.2 μ_B in $TbNi_4B$. We further refined the pattern by taking $\mu_{Ni}=0.0\ \mu_B$ and leaving the moments of the two rare earth site evolve separately in the refinement (modulus and direction). This led to the same modulus with a slightly different orientation of magnetic moments (8 deg difference) for the two terbium sites but this did not lead to any improvement of the reliability factors: $R_p=3.0\%$ and $R_I=6.0\%$ when $\theta_1=\theta_2$ and $R_p=3.1\%$ and $R_I=6.1\%$ when $\theta_1\neq\theta_2$. We thus considered that both terbium sites bear the same magnetic moment pointing in the same direction. Fig. 4 shows the final Rietveld refinement and Table 1 gathers the important parameters of this fit. Fig. 5 shows a schematic representation of the magnetic structure of $TbNi_4B$ at 1.6 K with the Tb moments oriented at $\theta=62$ deg from the c-axis. The saturation value $\mu_{Tb}=5.7\pm0.1\ \mu_B$ of the magnetic moment is well below the saturation moment of the free ion (9 μ_B). It is in good agreement with the published values of the saturation moment derived from magnetization measurements on polycrystals: 5.9 μ_B in Ref. [20] and 6.3 μ_B in Ref. [24]. The evolution with temperature of the moment modulus (μ_{Tb}) and angle (θ) are depicted in Fig. 6. Fitting a phenomenological power law to $\mu_{Tb}(T)$ between 1.6 K and 17.9 K yields $T_c=18.1\pm0.2$ K. This value is consistent the values of T_c reported in literature (19 K in Ref. [20] and 21 K in Ref. [24]). According to Liu et al. [56], a strong deviation of the experimental $\mu(T)$ from a Brillouin function [15] just below T_c indicates the possibility of a first order transition. Fig. 6 shows that $\mu_{Tb}(T)$ varies indeed more abruptly than the fitted Brillouin function, close to T_c. The transition to ferromagnetism thus appears to be a first order transition in $TbNi_4B$. The angle θ strongly varies when the temperature is increased from 1.6 K to T_c. It decreases from 62 deg (corresponding to the Tb moments only ~30 deg out of the (a, b) basal plane) to 0 deg at T_c which corresponds to the moment aligned with the c-axis.

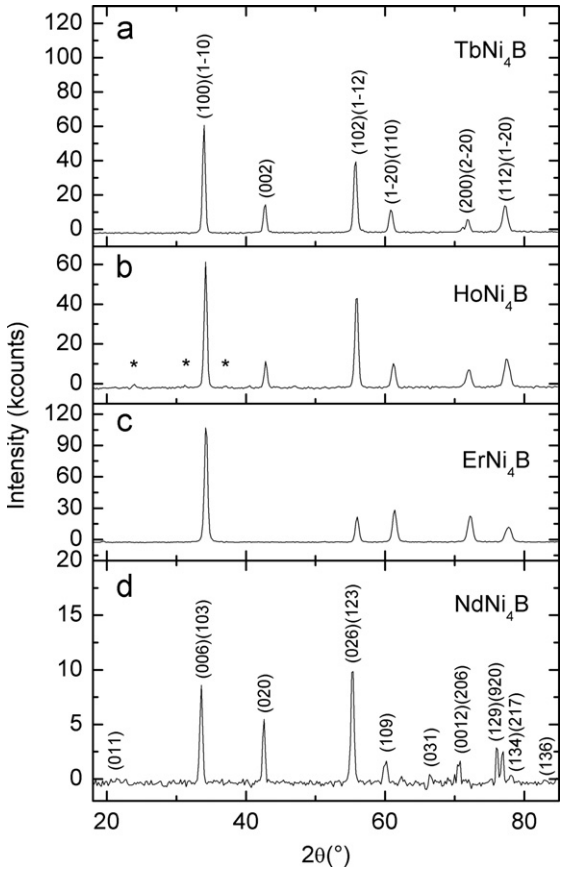

Fig. 3. Magnetic neutron difference patterns of $TbNi_4B$, $HoNi_4B$, $ErNi_4B$ and $NdNi_4B$. Panel a: 1.5 K pattern minus 33 K pattern in $TbNi_4B$, indexed by the hexagonal unit cell. Panel b: 1.6 K pattern minus 19 K pattern in $HoNi_4B$ indexed by the hexagonal unit cell; faint lines marked by asterisks ascribed to a magnetic secondary phase. Panel c: 1.5 K pattern minus 25 K pattern in $ErNi_4B$ indexed as well by the hexagonal unit cell. Panel d: 1.6 K pattern minus 24 K pattern in $NdNi_4B$. The Miller indexes correspond to the orthorhombic unit cell.

3.2.2. $HoNi_4B$

The most intense peaks of the difference pattern (1.6–19 K) of $HoNi_4B$ shown in Fig. 3b can be indexed with the $CeCo_4B$ unit cell

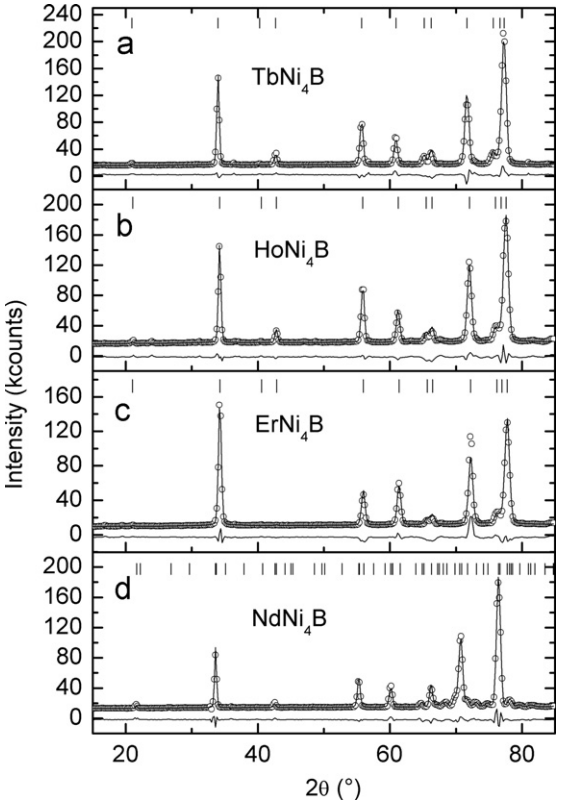

Fig. 4. Magnetic Rietveld refinement of the neutron pattern at 1.5–1.6 K. Panel a: $TbNi_4B$ (1.5 K); panel b: $HoNi_4B$ (1.6 K); panel c: $ErNi_4B$ (1.5 K); panel d: $NdNi_4B$ (1.6 K). The open circles are the experimental data, the passing-through line is the calculated pattern, the bottom line is the difference pattern (exp.−calc.) and the upper ticks are the Bragg angles.

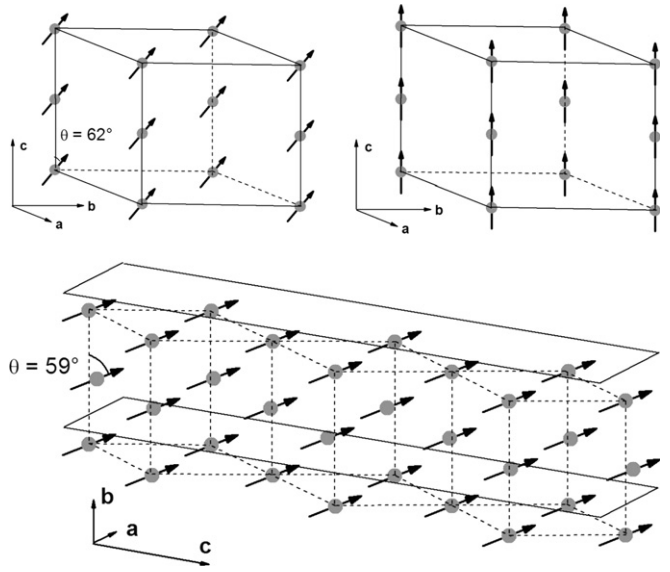

Fig. 5. Top left panel: schematic representation of the ferromagnetic structure in $TbNi_4B$ and $HoNi_4B$ at 1.6 K. The Tb or Ho moments are in the (a, c) plane and oriented at 62 deg from the *c*-axis. The gray spheres represent the Tb or Ho atoms. Top right panel: schematic representation of the ferromagnetic structure in $ErNi_4B$ at 1.6 K. The Er moments are parallel to the *c*-axis. Bottom panel: schematic representation of the ferromagnetic structure in $NdNi_4B$. The Nd moments are in the (b, c) plane of the orthorhombic structure and are oriented at 59 deg from the *b*-axis. The gray spheres represent the Nd atoms, the top and bottom planes represent the orthorhombic unit cell and the dashed lines represent the pseudo $CeCo_4B$ unit cells.

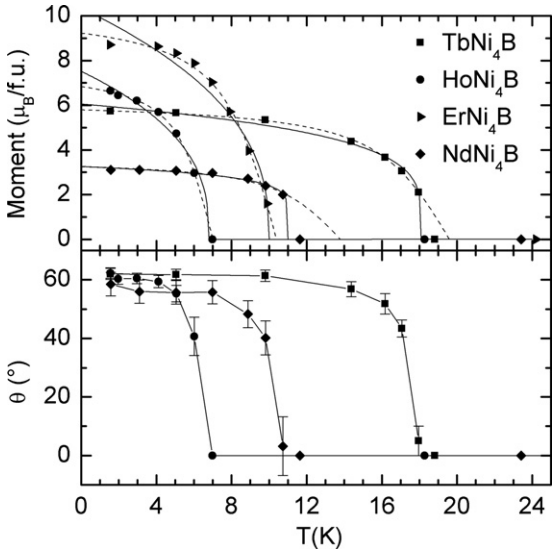

Fig. 6. Thermal variations of the magnetic moment μ_R (upper panel) and angle θ (lower panel) between the moment direction and the *c*-axis of the hexagonal unit cell (R=Tb, Ho, Er) or the *b*-axis of the orthorhombic unit-cell (R=Nd) in RNi_4B. For μ_R, the error bars are smaller than or as large as the symbols. In the upper panel, the μ_R=0 line is a guide to the eyes. The solid lines were obtained by fitting a phenomenological power law to the data while the dashed lines corresponds to a fit of a Brillouin function.

but very faint magnetic peaks marked with an asterix remain unindexed. These faint peaks do not correspond to any nuclear peaks of $HoNi_4B$ and do not appear at ~6–7 K=T_c like the $CeCo_4B$-like peaks but rather at 5K≠T_c. Moreover, we cannot index these peaks within the $Y_{0.9}Ni_{4.1}B$ [46] nor within the $Er_{0.9}Ni_{4.1}B$ [48] structures. This again strongly suggest that they belong to an unknown magnetic impurity phase and that the magnetic peaks of $HoNi_4B$ can be indexed using the $CeCo_4B$ unit cell. Similarly to $TbNi_4B$, the observation of (00l) peaks in the difference pattern indicates that in $HoNi_4B$, the moments make an angle θ with the *c*-axis at 1.6 K. Based on the results of $TbNi_4B$, we constrained the two rare earth sites to display the same moments and tested again the possibility of Ni moments. We obtained too small values for the Ni moments (μ_{Ni2c}=0±0.07 μ_B and μ_{Ni6i}=+0.2±0.07 μ_B) to be considered as genuine: here again, none of the nickel sites bears a "large" moment in $HoNi_4B$, if any. We obtained at T=1.6 K, μ_{Ho}=6.7(1) μ_B and θ=62 deg. Fig. 4 shows the Rietveld refinements and Table 1 gathers the relevant parameters to this fit finally described. Here again, the saturation value μ_{Ho}=6.7(1) μ_B of the magnetic moment is well below the saturation moment of the free Ho^{3+} ion (10 μ_B). It is however in line with the published values of the saturation moment derived from magnetization measurements: 7.5 μ_B in Ref. [20] and 7.8 μ_B in Ref. [24]. The evolutions with temperature of the moment modulus (μ_{Ho}) and angle (θ) with the *c*-axis of the $HoNi_4B$ hexagonal unit cell are displayed in Fig. 6. A power law fit of μ_{Ho}(T) between 1.6 K and 6.0 K yields T_c=6.2±0.2K, in agreement with the published values (6 K in Ref. [24]). Contrarily to $TbNi_4B$, there is no strong deviation between μ_{Ho}(T) and the fitted Brillouin function, indicating a second order transition. Similarly to $TbNi_4B$, the angle θ decreases from 62 deg at 1.6 K (μ_{Ho}~30 deg out of the (a, b) plane) to 0 deg at T_c (μ_{Ho}//*c*-axis).

3.2.3. $ErNi_4B$

Despite the uncertainty on the crystallographic structure of $ErNi_4B$, the magnetic neutron data were processed by taking the simple $CeCo_4B$-type of structure which can be currently considered as the best description for this crystal. This choice will further be supported by the simplicity of the arrangement of the Er moments and also by the simplicity of the magnetic structure in $NdNi_4B$ discussed hereafter. Indeed, despite the complexity of its crystallographic structure, $NdNi_4B$ displays a magnetic structure as simple as that of $TbNi_4B$. But given this uncertainty, we will neither discuss the presence of a moment on the Ni atoms nor the magnitude of the Er moments. The difference pattern (1.5–19 K) of $ErNi_4B$ is shown in Fig. 3. All these magnetic peaks could easily be indexed within the $CeCo_4B$ unit cell, indicating a ferromagnetic arrangement of the moment. Since no magnetic peak with (00l) indexes can be observed, the magnetic moments are oriented along the *c*-axis of the hexagonal $CeCo_4B$ structure type (Fig. 1). Based on the previous results obtained for $TbNi_4B$ and $HoNi_4B$, we performed a Rietveld refinement of the neutron pattern measured at 1.5 K assuming the same orientation and magnitude for the Er moments and no magnetic moments on the Ni sites. The result of this fit can be seen in Fig. 4 and the values of the resulting magnetic moment (μ_{Er}) and reliability factors are gathered in Table 1. The evolution of μ_{Er} with temperature is shown in Fig. 6 and a power law fit yields T_c=10.0±0.2 K. This value is slightly different from the 12 K reported in Ref. [24] but in close agreement with the 11 K reported in Ref. [22]. Similarly to $HoNi_4B$, there is no strong deviation between μ_{Er}(T) and the fitted Brillouin function, indicating a second order transition.

3.2.4. $NdNi_4B$

To be indexed, the magnetic difference pattern (1.6–25 K) required the orthorhombic cell [47] of the nuclear structure, as shown in Fig. 3. Here again, since there is no additional peaks other than those from the nuclear structure, the magnetic moments are ferromagnetically aligned. Based on the $TbNi_4B$ results, we considered that only the atoms of the 3 Nd sites (Nd1, Nd2, Nd3, same notations as in ref. [47]) and the atoms of the Ni1, Ni2, Ni3 and Ni7 nickel sites of the orthorhombic structure, which have an atomic environment similar to the atoms

of the Ni6i site of the $CeCo_4B$ approximate structure, bear a magnetic moment. We also forced the 3 Nd moments to be equal to one value as well as the 4 Ni moments to be equal to another value and globally all the moments to be parallel and contained in the (b, c) plane of the orthorhombic structure which is equivalent to the (c_0, a_0+b_0) plane of the $CeCo_4B$ structure. The low value of the Ni moment that we obtained ($\mu_{Ni}=-0.25\pm0.07\ \mu_B$) after Rietveld refinement again indicates that the Ni atoms do not carry a large moment, if any, in $NdNi_4B$. Similar to $TbNi_4B$, we refined the magnetic structure of $NdNi_4B$ with only the Nd atoms being magnetic. Relaxing the constraints $\mu_{Nd1}=\mu_{Nd2}=\mu_{Nd3}$ degraded the quality of the fit: $R_p=3.1\%$ and $R_I=9.0\%$ when $\mu_{Nd1}=\mu_{Nd2}=\mu_{Nd3}$ while $R_p=3.1\%$ and $R_I=10.0\%$ when $\mu_{Nd1}\neq\mu_{Nd2}\neq\mu_{Nd3}$. We thus kept the constraint $\mu_{Nd1}=\mu_{Nd2}=\mu_{Nd3}$ in all our subsequent refinements. Fig. 4 shows the final Rietveld refinement at $T=1.6$ K and the relevant parameters of this fit are also gathered in Table 1. Fig. 5 shows a schematic representation of the magnetic structure of $NdNi_4B$ at 1.6K with the Nd moments oriented at $\theta=59$ deg from the *b*-axis of the orthorhombic structure, which is parallel to the *c*-axis of the approximant hexagonal $CeCo_4B$ structure type. The moment orientation is thus very similar to that of Tb (62 deg) in $TbNi_4B$. The saturation value $\mu_{Nd}=3.1(1)\ \mu_B$ of the magnetic moment is very close to the saturation moment of the free ion ($3.3\ \mu_B$). It is at odds with the published values of the saturation moment derived from magnetization measurements: $1.6\ \mu_B$ in Ref. [20] and $1.7\ \mu_B$ in Ref. [24]. Fig. 6 shows the thermal variation of μ_{Nd} and θ, the angle with the *b*-axis of the orthorhombic structure. θ(T) decreases from $\theta=59$ deg to 0 deg when the temperature is varied from 1.6 K to $T_c=11$ K. μ_{Nd}(T) is well fitted by a power law which yields $T_c=11.0\pm0.2$ K, consistent with values from the literature ($T_c=11.7$ K in Ref. [20], $T_c=12$ K in Ref. [24]). Similarly to $TbNi_4B$, μ_{Nd}(T) varies more abruptly close to T_c than the fitted Brillouin function and this indicates the possibility of a first order transition in $NdNi_4B$. To summarize, $NdNi_4B$ magnetically behaves very similarly to $TbNi_4B$ despite the differences in their crystallographic structures.

4. Discussion

Table 2 shows a comparison between the Curie temperatures, the moment orientation (θ), the saturated moment per rare-earth atom derived from magnetization measurements (M_{sat}) and the rare-earth moment derived from neutron scattering experiments in RNi_5 and RNi_4B (R=Nd, Tb, Ho, Er) (μ_R). For both series of compounds, the experimental Curie temperature (T_c exp.) is compared to a Curie temperature (T_c DG) obtaining by scaling T_c of $GdNi_5$ (33 K in Ref. [12]) or $GdNi_4B$ (36 K in Ref. [22]) by the de Gennes factor $(g_J-1)^2J(J+1)$ where g_J is the Landé factor and J the total momentum quantum number of the rare earth R. Good agreement between the two temperatures would indicate a preponderance of the RKKY interaction over the CEF interactions. There is obviously a discrepancy between the experimental values and the scaled values, even for the heavy rare-earth and this is an indication of the importance of the CEF interactions over the RKKY interaction to determine the magnetic properties in both these series. The saturation moment M_{sat} is below the free rare earth ion value and this is another indirect indication of the importance of the CEF interactions. Since the spread between T_c exp. and T_c DG is similar in both series, a similar magnitude for the CEF interactions is also expected in both series. Usually a large discrepancy (~ factor of 2) between M_{sat} measured on a polycrystal and μ_R indicates a strong magneto-crystalline anisotropy because the magnetometer only measures a projection of the easy axis magnetization on the direction of the field (see for instance ref. [57]). This is effectively what is observed in $NdNi_4B$ but there is no large discrepancy between M_{sat} and μ_R in $TbNi_4B$ and $HoNi_4B$. These diverging results thus prevent a more detailed comparison between the intensity of CEF interactions in the RNi_4B and in the RNi_5 compounds.

Table 2 shows that there is also a strong analogy between the easy axis direction in the RNi_5 series and the RNi_4B series. At 1.5 K, the easy axis is the *c*-axis both in $ErNi_5$ and $ErNi_4B$ while it is the *a*-axis in RNi_5 (R=Nd, Tb, Ho) and it is only ~30° away from the (a, b) plane in RNi_4B (R=Nd, Tb, Ho). The easy and hard axes of magnetization are determined by the CEF interaction acting on the rare earth 4f shell. The point symmetry group of the R1a or R1b sites is 6/*mmm*. The corresponding CEF perturbing Hamiltonian acting on the ground state multiplet of the rare earth ions can thus be written [15] as:

$$H_{CEF}=\alpha_J V_2^0 O_2^0+\beta_J V_4^0 O_4^0+\gamma_J(V_6^0 O_6^0+V_6^6 O_6^6)$$

where the O_l^m are the Stevens operators, the V_l^m are the CEF parameters which depend on the surroundings and α_J, β_J, γ_J are the multipoles of the 4f shell or the "Stevens coefficients". In the RNi_5 series, the second order CEF parameter $\alpha_J V_2^0$ is three orders of magnitude larger than the fourth and sixth order terms (see for instance Ref. [6]) and the easy magnetization axis is fully determined by this former term and the sign of the second order Stevens coefficient of the rare-earth (α_J) across the series. Assuming $V_2^0<0$ in the RNi_5, the easy magnetization axis is the *a*-axis when $\alpha_J<0$ e.g. R=Nd, Tb, Ho and the easy magnetization axis is the *c*-axis when $\alpha_J>0$ e.g. R=Er. The situation is different in the RNi_4B (R=Nd, Tb, Ho, Er) since the easy axis at T_c is systematically the *c*-axis of the hexagonal $CeCo_4B$ structure, whatever the sign of the second order Stevens coefficient of the rare-earth (α_J) across the series. This shows the importance of fourth and sixth order terms of the Hamiltonian in the RNi_4B series to determine the easy axis at temperature close to T_c. The moment re-orientation towards a direction at 30 deg from the (a, b) plane which occurs in RNi_4B (R=Nd, Tb, Ho) when temperature is lowered below T_c indicates that the second order term of the CEF hamiltonian competes with the higher order terms and recovers some importance at lower temperature. This competition does not occur in

Table 2
Comparison of the experimental Curie temperature (T_c exp.) and Curie temperature obtained by de Gennes scaling (T_c DG), saturation magnetization (M_{sat}) derived from magnetometry (on single crystals for the RNi_5, on polycrystals for the RNi_4B series), moment per rare atom (μ_R) derived from neutron experiments and moment orientation (θ) in the RNi_5 and RNi_4B (R=Nd, Tb, Ho, Er) compounds.

Compound	RNi_5				RNi_4B			
R	Nd	Tb	Ho	Er	Nd	Tb	Ho	Er
T_c (K) exp.	7	23	4.5	10	11.0	18.1	6.2	10.0
T_c (K) DG	4	22	9	5	4	24	10	6
M_{sat} (μ_B)	2.9	8.4	9.2	7.8	1.6–1.7	5.9–7.3	7.5–7.8	5.0–7.7
μ_R (μ_B)	3.7	8.4	–	–	3.1	5.7	6.7	8.7
θ (deg)	90	90	90	0	59	62	62	0
Ref.	[8,11,13]	[6,10,11,14]	[6,11]	[5]	[23]	[20,24]	[20,24]	[22,24]

$ErNi_4B$ since the second order and higher order terms of the CEF hamiltonian favor the *c*-axis as the easy axis. No sign of a spin reorientation below T_c can be found in the various experimental data (magnetization, electronic transport, neutrons …) published in literature on the RNi_5 compounds. Such a phenomenon should not be confused with the spin re-orientation which occurs for instance in the RCo_5 compounds. In this last case, the spin re-orientation arises from the strong interaction between magnetic cobalt and rare earth atoms which tends to align the moments of the two sub-systems and the competition between the magneto-crystalline anisotropies of cobalt and rare earth atoms which tends to disalign the moments (see for instance [58,59]). The spin re-reorientation which occurs in the RNi_4B (R=Nd, Tb, Ho) is rather similar to what is seen in NdNi [60] where a reorientation of the Nd moments occurs when temperature is lowered below T_c because of the competition between the CEF terms. The RNi_4B series thus bears its originality in its complex CEF interactions leading to the spin re-orientation.

5. Summary

Our neutron data confirm that $NdNi_4B$ crystallizes in an orthorhombic structure while $TbNi_4B$ and $HoNi_4B$ crystallize in the classical $CeCo_4B$-type of structure. In the case of $ErNi_4B$, the proposed $Er_{0.9}Ni_{4.1}B$-type of structure cannot account for our data and the $CeCo_4B$ structure currently remains the best approximant. The RNi_4B (R=Nd, Tb, Ho, Er) are ferromagnetic and respectively order at 11.0, 18.1, 6.2 and 10.0 K. It is a first order transition for R=Nd, Tb and a second order transition for R=Ho, Er. The CEF interaction leads to a moment per rare earth atom smaller than the free rare earth ion and to magnetocrystalline anisotropy. The RNi_4B (R=Nd, Tb, Ho) display a spin re-orientation below T_c which arises from a competition between the second order term and the higher order terms of the CEF hamiltonian which cannot be neglected in this series.

Acknowledgments

The authors wish to thank J.L. Soubeyroux and O. Isnard for their technical help during the experiment at the ILL (Grenoble). They also acknowledge fruitful discussions with V. Paul-Boncour (ICMPE, Thiais) and G. André (LLB, Saclay).

References

[1] E.A. Nesbitt, H.J. Williams, J.H. Wernick, R.C. Sherwood, J. Appl. Phys. 33 (1962) 1674.
[2] K. Strnat, G.I. Hoffer, J.C. Olson, W. Ostertag, J.J. Becker, J. Appl. Phys. 38 (1967) 1001.
[3] J.H.N. Van Vucht, F.A. Kuijpers, H.C.A.M. Bruning, Philips Res. Rep. 25 (1970) 133.
[4] F.A. Kuijpers, H.H. Van Mal, J. Less-Common Met. 23 (1971) 395.
[5] P. Escudier, D. Gignoux, D. Givord, R. Lemaire, A.P. Murani, Physica B+C 86 (1977) 197.
[6] D. Gignoux, A. Nait-Saada, R. Perrier de la Bâthie, J. Phys. Colloq. 40 (1979) C5.
[7] R. Ballou, V.M.T.S. Barthem, D. Gignoux, Physica B+C 149 (1988) 340.
[8] V.M.T.S. Barthem, D. Gignoux, A. Nait-Saada, D. Schmitt, A.Y. Takeuchi, J. Magn. Magn. Mater. 80 (1989) 142.
[9] V.M.T.S. Barthem, D. Gignoux, D. Schmitt, G. Creuzet, J. Magn. Magn. Mater. 78 (1989) 56.
[10] C. Carboni, D. Gignoux, A. Tari, Phys. Rev. B 52 (1995) 9486.
[11] L. Morellon, P.A. Algarabel, A. del Moral, D. Gignoux, D. Schmitt, J. Magn. Magn. Mater. 153 (1996) 17.
[12] W.E. Wallace, M. Aoyagi, Monatsh. Chem. 102 (1971) 1455.
[13] J.I. Espeso, N. Marcano, A. Señas, J.A. Blanco, M. Reiffers, J.C.Gomez Sal, J. Magn. Magn. Mater. 226–230 (2001) 1150, Part 2.
[14] R. Lizarraga, A. Bergman, T. Björkman, H.-P. Liu, Y. Andersson, T. Gustafsson, A. G. Kuchin, A.S. Ermolenko, L. Nordström, O. Eriksson, Phys. Rev. B 74 (2006) 094419.
[15] D. Gignoux, in: E. Trémolet de Lacheisserie (Ed.), Magnétisme, vol. 1, Presses Universitaires de Grenoble, Grenoble, 1999.
[16] S. Lee, A. Podlesnyak, K. Prokes, V. Sikolenko, A. Ermolenko, E. Gerasimov, Y. Dorofeev, A. Vokhmyanin, J. Park, A. Pirogov, JETP Lett. 82 (2005) 34.
[17] V.M.T.S. Barthem, E.A.M. daGama, J. Phys.-Condens. Matter 9 (1997) 7609.
[18] F.E. Spada, H. Oesterreicher, R.C. Bowman, M.P. Guse, Phys. Rev. B 30 (1984) 4909.
[19] N.M. Hong, N.P. Thuy, G. Schaudy, T. Holubar, G. Hilscher, J.J.M. Franse, J. Appl. Phys. 73 (1993) 5698.
[20] N.M. Hong, T. Holubar, G. Hilscher, M. Vybornov, P. Rogl, IEEE Trans. Magn. 30 (1994) 4966.
[21] R. Nagarajan, L.C. Gupta, C. Mazumdar, Z. Hossain, S.K. Dhar, C. Godart, B. D. Padalia, R. Vijayaraghavan, J. Alloys Compd. 225 (1995) 571.
[22] C. Mazumdar, Ph.D. Thesis, Indian Institute of Technology, Bombay, 1995.
[23] T. Tolinski, A. Kowalczyk, A. Szlaferek, M. Timko, J. Kovac, Solid State Commun. 122 (2002) 363.
[24] T. Tolinski, A. Kowalczyk, A. Szlaferek, B. Andrzejewski, J. Kovac, M. Timko, J. Alloys Compd. 347 (2002) 31.
[25] T. Tolinski, A. Kowalczyk, V. Ivanov, Phys. Status Solidi B 240 (2003) 153.
[26] T. Tolinski, B. Andrzejewski, A. Kowalczyk, Z. Trybula, J. Baszynski, J. Magn. Magn. Mater. 267 (2003) 402.
[27] T. Tolinski, Mod. Phys. Lett. B 21 (2007) 431.
[28] C. Mazumdar, R. Nagarajan, L.C. Gupta, B.D. Padalia, R. Vijayaraghavan, Appl. Phys. Lett. 77 (2000) 895.
[29] M. Pugaczowa-Michalska, G. Chelkowska, A. Kowalczyk, Acta Phys. Pol. A 104 (2003) 487.
[30] M. Pugaczowa-Michalska, T. Tolinski, A. Kowalczyk, G. Chelkowska, Czech. J. Phys. 54 (2004) D347.
[31] M. Pugaczowa-Michalska, A. Kowalczyk, G. Chelkowska, T. Tolinski, J. Alloys Compd. 385 (2004) 44.
[32] T. Tolinski, A. Kowalczyk, G. Chelkowska, Phys. Lett. A 308 (2003) 75.
[33] T. Tolinski, M. Pugaczowa-Michalska, G. Chelkowska, Phys. Status Solidi B-Basic Solid State Phys. 242 (2005) 474.
[34] C. Lazar, E. Burzo, M. Neumann, J. Optoelectron. Adv. Mater. 10 (2008) 780.
[35] P. Vlaic, N. Bucur, C. Lazar, E. Burzo, J. Optoelectron. Adv. Mater. 8 (2006) 490.
[36] E. Burzo, Rom. Rep. Phys. 59 (2007) 337.
[37] R. Nagarajan, C. Mazumdar, Z. Hossain, S.K. Dhar, K.V. Gopalakrishnan, L.C. Gupta, C. Godart, B.D. Padalia, R. Vijayaraghavan, Phys. Rev. Lett. 72 (1994) 274.
[38] R.J. Cava, H. Takagi, H.W. Zandbergen, J.J. Krajewski, W.F. Peck, T. Siegrist, B. Batlogg, R.B. Van Dover, R.J. Felder, K. Mizuhashi, J.O. Lee, H. Eisaki, S. Uchida, Nature 367 (1994) 252.
[39] C. Mazumdar, R. Nagarajan, C. Godart, L.C. Gupta, M. Latroche, S.K. Dhar, C. Lévy-Clément, B.D. Padalia, R. Vijayaraghavan, Solid State Commun. 87 (1993) 413.
[40] T. Tolinski, J.C. Cezar, H. Wende, A. Kowalczyk, K. Baberschke, Acta Phys. Pol. A 115 (2009) 129.
[41] C. Mazumdar, Z. Hu, G. Kaindl, Physica B 259&261 (1999) 89.
[42] T. Tolinski, A. Kowalczyk, M. Pugaczowa-Michalska, G. Chelkowska, J. Phys., Condens. Matter 15 (2003) 1397.
[43] K. Niihara, Y. Katayama, S. Yajima, Chem. Lett. (1973) 613.
[44] Y.B. Kuz′ma, M.P. Khaburskaya, Izv. Akad. Nauk SSSR Neorg. Mater. 11 (1975) 1893.
[45] Y.B. Kuz′ma, N.S. Bilonizhko, Izv. Akad. Nauk SSSR Neorg. Mater. 7 (1971) 620.
[46] A. Belger, G. Zahn, B. Wehner, P. Paufler, G. Graw, G. Behr, J. Alloys Compd. 283 (1999) 26.
[47] P.S. Salamakha, O. Sologub, C. Mazumdar, E. Alleno, H. Noël, M. Potel, C. Godart, J. Alloys Compd. 351 (2003) 190.
[48] Y.B. Kuz′ma, V. Babizhetskyj, I. Veremchuk, N. Chaban, J. Solid State Chem. 177 (2004) 425.
[49] P.S. Salamakha, O.L. Sologub, J.R. Hester, C. Rizzoli, A.P. Goncalves, M. Almeida, J. Alloys Compd 439 (2007) 162.
[50] J. Rodriguez-Carvajal, Physica B 192 (1993) 55.
[51] ⟨http://www.ncnr.nist.gov/instruments/bt1/neutron.html⟩.
[52] G.V. Chernyak, N.F. Chaban, Y.B. Kuz′ma, Inorg. Mater. 18 (1982) 590.
[53] I.B. Gubich, Y.B. Kuz′ma, N.F. Chaban, Inorg. Mater. 29 (1993) 1104.
[54] S. Geupel, A. Belger, P. Paufler, G. Graw, Z. Kristallogr.-New Crys. Struct. 215 (2000) 481.
[55] I.B. Hubych, Visn. L′viv. Derzh. Univ. (Ser. Khim.), 1991, p. 31.
[56] X.B. Liu, D.H. Ryan, Z. Altounian, J. Magn. Magn. Mater. 270 (2004) 305.
[57] P. Bonville, J.A. Hodges, Z. Hossain, R. Nagarajan, S.K. Dhar, L.C. Gupta, E. Alleno, C. Godart, Eur. Phys. J. B 11 (1999) 377.
[58] B. Decrop, J. Déportes, R. Lemaire, J. Less-Common Met. 94 (1983) 199.
[59] Z. Tie-song, J. Han-min, G. Guang-hua, H. Xiu-feng, C. Hong, Phys. Rev. B 43 (1991) 8593.
[60] G. Fillion, D. Gignoux, F. Givord, R. Lemaire, J. Magn. Magn. Mater. 44 (1984) 173.